

# Structural Forecasting for Short-term Tropical Cyclone Intensity Guidance

TREY MCNEELY,<sup>a</sup> PAVEL KHOKHLOV, NICCOLÒ DALMASSO,<sup>b</sup> KIMBERLY M. WOOD,<sup>c</sup> AND ANN B. LEE<sup>a</sup>

<sup>a</sup> *Carnegie Mellon University Department of Statistics and Data Science*

<sup>b</sup> *J.P. Morgan AI Research*

<sup>c</sup> *Mississippi State University Department of Geosciences*

**ABSTRACT:** Geostationary satellite (GOES) imagery provides a high temporal resolution window into tropical cyclone (TC) behavior. We present a new method for probabilistic forecasting not only of TC intensity but also TC convective structure as revealed by GOES. This paper describes a prototype model based solely on observed infrared imagery and past operational intensity estimates. These structural forecasts simulate the spatio-temporal evolution of the radial profiles of cloud-top temperatures over the subsequent 12 hours. Our structural forecasting pipeline applies a Deep Autoregressive Generative Model (PixelSNAIL) to create probabilistic forecasts of the evolution of these functions over time. A standard convolutional neural network (trained for “nowcasting”, or predicting the current state based on past states and current features) is then applied to simulated structural trajectories to predict intensities at lead times of 6 to 12 hours.

Intensity guidance from our prototype model achieves a marginally higher error than the National Hurricane Center’s official forecasts. However, our prototype model does not account for environmental factors such as vertical wind shear and sea surface temperature. We demonstrate that it is possible to reasonably predict short-term evolution of TC convective structure as depicted by infrared imagery, producing interpretable structural forecasts that may be valuable for TC operational guidance.

**SIGNIFICANCE STATEMENT:** This work presents a new method for probabilistic forecasts of not only tropical cyclone intensity but also their convective structure as revealed by satellite imagery. Intensity forecasts are ultimately issued by human forecasters, and interpretable structural forecasts can provide helpful guidance to forecasters regarding potential short-term TC evolution. The performance of the presented prototype model (which does not yet incorporate any atmospheric conditions) suggests that future iterations which incorporate atmospheric conditions could support improvements to current official forecasts and at the same time provide additional information on the joint evolution of storm intensity and structure up to 12 hours into the future.

## 1. Introduction

Tropical cyclones (TCs) are powerful, organized systems which pose a major risk to coastal populations. Though many statistical models exist that provide forecast guidance on future TC intensity change (e.g., the Statistical Hurricane Intensity Prediction Scheme [SHIPS]; DeMaria and Kaplan 1999), direct measurement of most predictors such as relative humidity or vertical wind shear used in such models is impossible due to the development of TCs over open ocean far from land-based observing networks (Gray 1979). Many predictors must be inferred through a combination of remote observation and dynamic models of ocean and atmospheric behavior.

Infrared (IR;  $10.3\mu\text{m}$ ) imagery from geostationary (Geo) satellites such as the Geostationary Operational Environmental Satellites (GOES) provides one of the few regular high-resolution observations of TC behavior over the open ocean with a historical record spanning decades (Knapp and Wilkins 2018; Janowiak et al. 2020). Furthermore, modern Geo IR platforms such as GOES-16 provide observations at even greater spatial and temporal resolution (Schmit et al. 2017). Since cloud-top temperature is related to cloud-top height, low IR temperatures tend to indicate higher cloud tops and thus stronger convection, and convective structures are known to be related to TC intensity (Dvorak 1975; Olander and Velden 2007).

In light of this growing record of satellite observations, a broad array of recent works have explored the wealth of information contained in the *spatio-temporal* structure of Geo IR imagery. The Dvorak technique and more recent Advanced Dvorak Technique (ADT) have long related Geo IR imagery to TC intensity (Dvorak 1975; Olander and Velden 2007), and more recent work has leveraged neural networks to improve the nowcasting accuracy of the ADT (AI enhanced Dvorak Technique; Olander and Velden 2019). Here, we define “nowcasting” as predicting the current state, such as TC intensity, based on past states and current features. Spatial analyses of IR imagery have improved forecasts of TC eye formation, a process related to intensification (DeMaria 2015; Knaff and DeMaria 2017). The deviation angle variance (DAV) technique, a measure of convective organization in IR imagery, contains valuable information for short-term TC intensity guidance (Hu et al. 2020). The shape and evolution of Geo IR radial profiles

---

*Corresponding author:* Ann B. Lee, annlee@stat.cmu.edu

(e.g., symmetric eyewall slope) is known to relate to intensity and intensity change respectively (Sanabia et al. 2014; McNeely et al. 2020). In this work, we utilize the *evolution over time* of radial profiles (see Figure 1) to jointly forecast short-term structural and intensity changes. We leverage deep auto-regressive (AR) generative models to construct *interpretable and high-resolution* structural probabilistic forecasts, which display entire functions rather than time series of thresholded quantities, such as pixel counts beneath a given temperature threshold.

Concurrent with the rise of high-resolution Geo IR imagery is the growing application of convolutional neural networks (CNNs), powerful tools for performing prediction tasks with images as input. Predicting TC intensity from Geo IR data is an obvious candidate application; indeed, there are dozens of such works in the machine learning literature applying CNNs to this problem, including Pradhan et al. (2017); Combinido et al. (2018); Lee et al. (2019); Tian et al. (2020); Wang et al. (2020); and Zhang et al. (2021). These models achieve reasonable forecast accuracy via the traditional machine learning framework, wherein a CNN mapping Geo IR data and other features to intensity is trained to optimize prediction performance. Explainable AI approaches may then use methods such as layer-wise relevance propagation, salience maps, and activation maps to better understand *how* the model produced its point estimate (McGovern et al. 2019; Ebert-Uphoff and Hilburn 2020). For an example of explainable CNN-based TC intensity forecasting in the meteorological literature, see Griffin et al. (2022).

Our proposed pipeline takes a different approach to explainability—one which is still compatible with the above tools for insight into the relationships leveraged by CNNs. Our approach (i) utilizes a dimensionality-reducing functional transformation of IR imagery prior to analysis, and (ii) provides simulated 12 hour forecasts of these functional summaries in addition to point-estimates of intensity.

First, we extract *scientifically-motivated functional features*, reducing the dimension of the problem (from 2-D images over time to 1-D functions over time) in a directly interpretable summary, rather than relying on the CNN to extract salient features from (high-dimensional and low-sample size) raw Geo IR imagery on its own. These rich summary functions are derived from the ORB suite: Organization (e.g., DAV as a function of radius), Radial structure (e.g., the radial profiles examined in this work), and Bulk morphology (e.g., pixel counts as a function of a temperature threshold). Temporal sequences of radial profiles are highly relevant to both intensity and intensity change (Sanabia et al. 2014; McNeely et al. 2020, 2022). Temporal changes in these sequences of profiles are easy to visualize via static Hovmöller diagrams, which are more readily digestible by users than inferring temporal patterns from animations of satellite imagery.

Second, we provide a *structural forecast*, a prediction of possible TC convective evolution, rather than directly predicting future intensity from past structure. These structural forecasts play a role analogous to albeit simpler than numerical weather prediction, which predicts environmental variables from current conditions via the governing equations. Our novel approach to intensity guidance via Geo IR imagery results in interpretable intensity guidance such as “our model predicts stronger intensification than SHIPS due to the simulated emergence of an eye-eyewall structure in the next 12 hours.” Though methods such as layer-wise relevance propagation can provide further insight into the CNN’s use of structural forecasts, the IR structural forecasts themselves are the core of our proposed intensity guidance pipeline.

Figure 2 shows a schematic diagram of the structural forecasting to intensity guidance pipeline. There are three main steps outlined in Section 3:

- (a) *Structural trajectories via ORB*. First, we apply the ORB framework (McNeely et al. 2019, 2020) to observed IR imagery to create a “structural summary” (as in Figure 1) of the spatio-temporal evolution of the present and recent past TC structure.
- (b) *Structural forecasting via deep AR generative models*. Next, we propagate the “observed structure” 6 to 12 hours forward in time via a deep pixel-autoregressive model (Equation 1), which stochastically simulates possible trajectories of radial profiles.
- (c) *Nowcasting TC intensity via convolutional neural nets*. Finally, we input the observed structure, the forecasted structure, and TC intensity into a “nowcasting” model to predict the current intensity; we choose convolutional neural nets (CNNs) because they are easy to train and commonly used for image data. By forecasting  $\mathbf{S}_{<t}$ , we can transfer the nowcasting model from a nowcast for time  $t$  to a forecast at time  $t+6$  hours.

Section 4 details the results of our prototype forecasting pipeline. The final Geo IR-based TC intensity guidance provides inherent measures of uncertainty and—in the simulated future structure of the TC—insight into the expected TC behavior which leads to a given forecast. The results in this work use proof-of-concept structural forecasting and nowcasting models which rely solely on persistence predictors (i.e., past intensity) together with radial profiles; no environmental factors such as vertical wind shear or ocean heat content are included at this time. We demonstrate that a purely autoregressive prototype achieves a useful degree of forecasting accuracy, but the inclusion of environmental factors will be necessary for this pipeline to achieve its full potential.

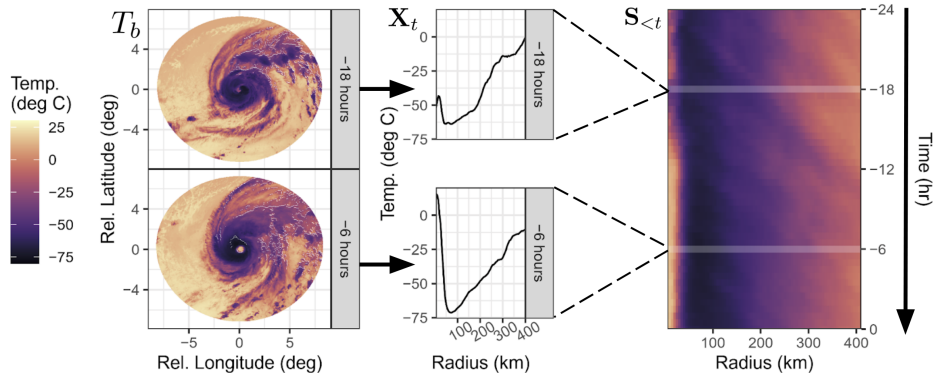


FIG. 1. **Evolution of TC IR Imagery as Structural Trajectories.** The raw data at each time  $t$  is a sequence of TC-centered cloud-top temperature images from GOES. We quantify the image at time  $t$  by its radial profile ( $X_t$ ). The sequence of consecutive radial profiles, sampled every 2 hours, defines a *structural trajectory* or Hovmöller diagram ( $S_{<t}$ ).

## 2. Data

This model relies on two types of observations: sequences of Geo IR imagery captured by GOES satellites and TC information provided by NOAA’s Hurricane Database 2 (HURDAT 2; Landsea and Franklin 2013) or the Naval Research Laboratory’s Automated Tropical Cyclone Forecast (ATCF) operational “B-deck” files (Sampson and Schrader 2000). For training, we use HURDAT2 TC intensity estimates. However, for forecasting, we use operational TC intensity estimates from the B-deck files to evaluate the model’s performance under real-time conditions.

GOES  $10.3\mu\text{m}$  IR imagery is available through NOAA’s Merged IR (MERGIR) database (Janowiak et al. 2020) at 30-minute $\times$ 4-km resolution over both the North Atlantic (NAL) and Eastern North Pacific (ENP) basins from 2000–present. Every thirty minutes during the lifetime of a TC, we download a  $\sim 2,000\text{ km}\times 2,000\text{ km}$  “stamp” of IR imagery centered on the TC location. Figure 1 (left) shows two such stamps after an 800-km radius mask is applied. For this work, we sample the 30-minute data at a lower 2-hour resolution because of periodic corruption of the imagery in the MERGIR database (Liu 2021).

During training, we linearly interpolate TC location and intensity from HURDAT2 to obtain locations and intensities for non-synoptic times; however, model assessment is restricted to synoptic times. We include TC lifetimes between the first synoptic time at which intensity reaches at least 35 kt and the last synoptic time at which intensity is at least 35 kt. While the HURDAT2 database gives a post-season best estimate of TC intensities to serve as a ground truth during training and for validation, forecasts should be based on operationally-available quantities; we thus draw past intensity values (persistence predictors) from the ATCF database of *operational* intensities during forecasting. That is, the model has access only to B-deck inputs

when forecasting, and its forecasts are graded against the HURDAT2 best track record.

Finally, we draw on the SHIPS developmental database’s 200-850-hPa vertical wind shear values calculated within a 200-800-km annulus from the TC center to use during model validation due to the impact of shear on TC convective structure (DeMaria 2018). We also use the NHC official forecast validation files to assess our model’s performance against that baseline, as in Tables 2 and 3 (NHC 2022).

## 3. Methods

As outlined in Figure 2, we first construct a summary of IR structural evolution (**a**; Section 3a). We then train a stochastic autoregressive model, which is an explicit likelihood model (of structural trajectories) that we can use to simulate probable IR structural evolution (**b**; Section 3b). Finally, we combine observed and forecasted structure with observed intensity to provide interpretable short-term intensity guidance, based solely on Geo IR imagery and operational intensity estimates (**c**; Section 3c).

### a. Structural Trajectories via ORB

Operational forecasting of TC intensity is a human-in-the-loop process and thus places a premium on guidance interpretability. In this spirit, the ORB framework (Organization, Radial structure, Bulk morphology) summarizes 2-D imagery via continuous 1-D functions to enable static visualization of spatio-temporal patterns in TC development via Hovmöller diagrams (Hovmöller 1949). Our past work focused on the rich quantification of spatial information in Geo IR imagery (McNeely et al. 2019, 2020). More recently, we demonstrated the value of *temporal* patterns in ORB functions (McNeely et al. 2022), specifically the radial profile.

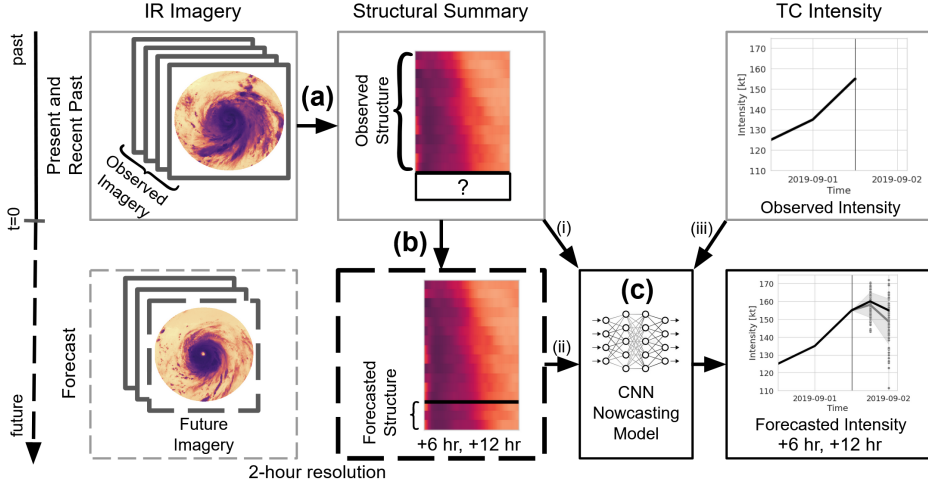


FIG. 2. **TC Intensity Guidance via Structural Forecasting.** Outline of the structural forecasting to intensity guidance pipeline. (a) ORB functions are used to quantify the evolution of spatio-temporal convective structure. (b) We generate structural forecasts by projecting the ORB functions into the future via a deep autoregressive model. (c) A CNN nowcasting model then generates forecasted intensities at +6 to +12 hours from three sources of inputs: (i) observed structure, (ii) forecasted structure, and (iii) observed storm intensity.

The radial profile  $\bar{T}(r) = \frac{1}{2\pi} \int_0^{2\pi} T_b(r, \theta) d\theta$  captures the structure of cloud-top brightness temperatures ( $T_b$ ) as a function of radius  $r$  from the TC center and serves as an easily interpretable description of the depth and location of convection near the TC core (Sanabia et al. 2014; McNeely et al. 2020). The radial profiles are computed at 5-km resolution from 0-400 km ( $d = 80$ ) (Figure 1, center); we denote the summary of convective structure at each time  $t$  by  $\mathbf{T}_t$ . The *structural trajectory*  $\mathbf{S}_{<t} = (\mathbf{T}_t, \mathbf{T}_{t-1}, \dots, \mathbf{T}_{t-48})$  is then defined as the 24-hour sequence of present and 48 preceding radial profiles. We visualize such a trajectory with a Hovmöller diagram (see Figure 1, right).

McNeely et al. (2022) demonstrated a relationship between TC intensity change and Hovmöller diagrams of radial profiles. However, the radial profile, if averaged over all angles, will disregard asymmetry within the original 2-D images, which led to poor method performance for cases with high vertical wind shear, such as 2017’s Hurricane Jose. In this work, we will instead compute a separate radial profile for each geographic quadrant (NE, NW, SE, SW) to capture asymmetries via the differences between quadrants. We use geographic quadrants instead of motion-relative or shear-relative quadrants because the directions of motion and shear are unstable when the magnitudes of the vectors are small.

### b. Structural Forecasting via Deep Autoregressive Generative Model

The crucial step in our guidance framework is the propagation of radial profiles into the near future. The Hovmöller diagram captures the spatio-temporal evolution of the TC over an extended period of time; that is, we can summarize TC development by an easily-interpretable image. By

treating the structural trajectory as an image, where the y-axis corresponds to the passage of time, forecasting radial profiles becomes equivalent to an image completion problem. That is, we predict the missing pixels at the bottom of an image (forecasted structure) given those at the top (observed structure). Image completion is an active research area in machine learning; here we focus on a state-of-the-art model in the class of pixel-autoregressive models (Van Oord et al. 2016).

Pixel-autoregressive models impose an ordering on the pixels of an image, such as a raster-scan ordering (left-to-right, top-to-bottom). Let each pixel in a 4-quadrant radial profile trajectory be represented by  $\mathbf{x}_i := (x_{i1}, x_{i2}, x_{i3}, x_{i4})$ , where  $i$  is the index in the raster scan. The pixel-AR approach factors the joint distribution of pixel values in the image as a product of conditionals,

$$p(\mathbf{x}_1, \dots, \mathbf{x}_n) = \prod_{i=1}^n p(\mathbf{x}_i | \mathbf{x}_{i-1}, \dots, \mathbf{x}_1), \quad (1)$$

where the probability of each pixel value is conditioned on all previous pixels in the raster scan. Then, to generate a new radial profile, one simulates repeatedly from  $p(\mathbf{x}_i | \mathbf{x}_{i-1}, \dots, \mathbf{x}_1)$ ; due to the raster-scan ordering, the distribution of a given pixel is not influenced by elements further down the sequence, hence enforcing causality.

The challenge of how to estimate the conditional likelihoods  $p(\mathbf{x}_i | \mathbf{x}_{i-1}, \dots, \mathbf{x}_1)$  has given rise to the many flavors of pixel-autoregressive models, including PixelRNN (Van Oord et al. 2016), PixelCNN (Van den Oord et al. 2016), PixelCNN++ (Salimans et al. 2017), and PixelSNAIL (Chen et al. 2018). This work utilizes the last model, PixelSNAIL. There are two main ingredients in

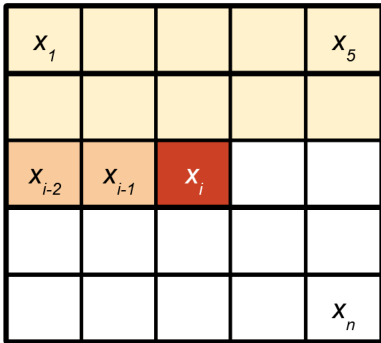


FIG. 3. **Masking in Pixel Autoregression.** Illustration of raster-scan ordering and the causal masking. Convolutions at index  $i$  only have access to pixel values in previous rows (earlier time points, color coded by yellow), and pixel values in the same row but to the left of pixel  $x_i$  (same time point, color coded by orange).

the model: (i) causal convolution and (ii) self-attention. Causal convolution utilizes the same convolutional feature extraction outlined in Section c but masks each convolution so that each element in the raster sequence only receives information from previously generated sequences (e.g., Figure 3). Purely convolutional models, however, are restricted to small neighborhoods of pixels, leading to only a finite receptive field (area of the source image involved in a given convolution), and thus struggle with long-range dependencies in the conditional  $p(\mathbf{x}_i|\mathbf{x}_{i-1}, \dots, \mathbf{x}_1)$ . Pixel-SNAIL, on the other hand, features a self-attention mechanism that leads to unbounded receptive fields with pin-pointed access to information far away in the sequence; see Chen et al. (2018) for details on the PixelSNAIL architecture.

To ensure that cloud-top temperatures remain bounded, we rescale the data to the range  $\mathbf{X} \in (0, 1)^4$  and work in the logit-transformed space,  $\mathbf{Z} = \log(\mathbf{X}/(1 - \mathbf{X}))$ ; while values of  $\mathbf{Z}$  are unbounded,  $\mathbf{X}$  remains bounded in  $(0, 1)^4$  and are then transformed back to the temperature range observed in the training data. We model the density  $p(\mathbf{z}_i|\mathbf{z}_{i-1}, \dots, \mathbf{z}_1)$  as 4 independent mixtures of logistic distributions, one for each quadrant. That is, for pixel  $i$  in quadrant  $q$ ,

$$p(Z_{iq}|\mathbf{Z}_{i-1}, \dots, \mathbf{Z}_1) = \sum_{k=1}^K \pi_{qk} f(z_{iq}; \mu_{qk}, s_{qk}) \quad (2)$$

$$\text{where } f(z_{iq}; \mu_{qk}, s_{qk}) = \frac{g_{qk}(z)}{s_{qk}(1 - g_{qk}(z))^2}, \quad (3)$$

$$g_{qk}(z) = \exp(-(z - \mu_{qk})/s_{qk}), \quad (4)$$

$$\text{and } \sum_{k=1}^K \pi_{qk} = 1. \quad (5)$$

Thus, with 4 quadrants and  $K$  mixture components, the distribution  $p(\mathbf{z}_i|\mathbf{z}_{i-1}, \dots, \mathbf{z}_1)$  has  $4(3K - 1)$  parameters: a mean  $\mu$ , a scale  $s$ , and a mixture coefficient  $\pi$  for each

quadrant, with the constraint in Equation 5 that the mixture coefficients in each quadrant sum to one. With  $K = 3$  mixture components, this results in 32 parameters total. Each draw from the distribution is transformed back to the bounded space via the relationship  $\mathbf{X} = \frac{1}{1 + \exp(-\mathbf{Z})}$ , then rescaled to the range of values observed in the input radial profiles.

This autoregressive model enables stochastic simulation of structural trajectories based on Geo IR persistence. For a given synoptic time, we can simulate many trajectories from the observed history and then feed each potential trajectory through the nowcasting model to obtain the associated intensity guidance. Via multiple simulations per forecast time, an ensemble forecast provides a measure of uncertainty in both structural trajectories and intensities while also allowing insight into cases where the model over- or under-estimates intensity. For example, overestimates may be caused by too-low profile temperatures or overestimated symmetry between quadrants.

The structural forecasting model is trained on TCs from 2000-2012, with 2013-2020 withheld for testing. We train the model using input radial profiles calculated every 2 hours but test on synoptic times. Because AR models are likelihood-based, we can directly calculate and minimize the negative log-likelihood (NLL), a measure of the model's ability to generalize well on withheld data.

### c. Nowcasting TC Intensity via Convolutional Neural Networks

Traditional linear models are attractive for reasons of interpretability and good performance in low sample size settings. However, linear models often struggle to capture the complex, time-varying processes which drive TCs. It is also unclear how to include the radial profile Hovmöller diagrams as inputs to a linear model without sacrificing interpretability. In this work, we instead consider a simple convolutional neural network to map observed IR trajectories ( $\mathbf{S}_t$ ) to current intensities ( $Y_t$ ). Because we treat time as a spatial dimension in these diagrams and a structural trajectory is represented as an image, a CNN will leverage both spatial and temporal patterns in the data.

CNNs operate by two main elements: convolutional layers and fully-connected layers. The convolutional layers first convolve each layer (here, each quadrant) with a library of filters (i.e., matrices whose entries are learned parameters); some of these filters may resemble familiar matrices, such as gradient approximators (e.g., Sobel matrices). After each convolutional layer, the image is pooled to reduce the image size and increase the receptive field of the next set of convolutions. In the final step, the results of all convolutions are passed into a fully-connected layer which approximates the relationship between the convolutional feature map and the response.

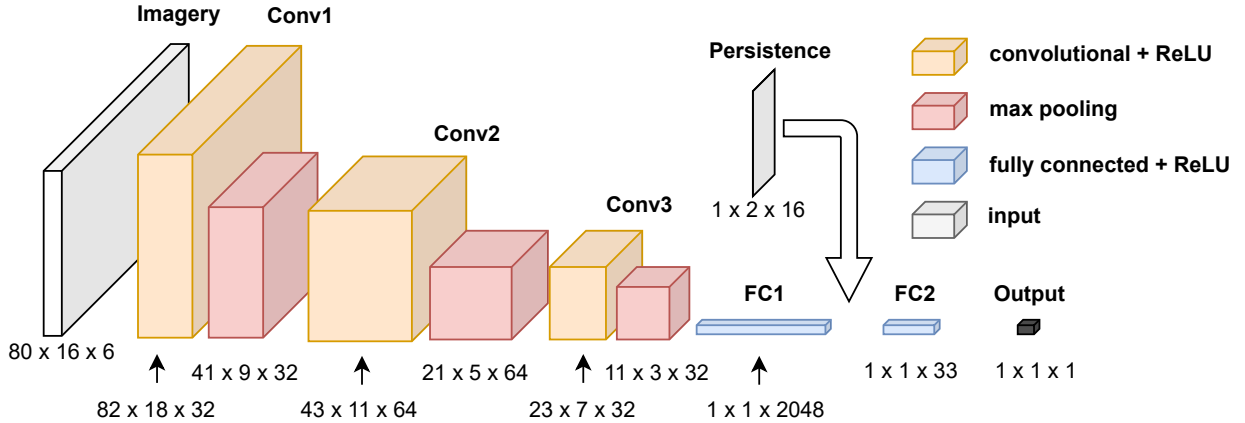


FIG. 4. **Nowcasting Model Architecture.** The convolutional neural network used for nowcasting consists of 3 convolution-max pool layer pairs (Conv#), fully connected layers (FC#), and a concatenation with persistence features between regressions.

We augment the traditional CNN in two ways. First, we add two layers which encode the radial and temporal location of pixels within the image; regular CNNs are translation invariant, whereas patterns in TCs have different meaning depending on their location and time of occurrence (corresponding to column versus row index, respectively, in the Hovmöller diagram). Second, we augment the model output with relevant TC persistence features (intensities and intensity changes up to 6 hours prior to time  $t$ ,  $Y_{t-30}, \dots, Y_{t-6}, \Delta Y_{t-30}, \dots, \Delta Y_{t-6}$ ) before passing them to a second fully-connected layer. The final model is then

$$Y_t = f_{\text{nowcast}}(\mathbf{S}_{<t}, Y_{t-6}, \dots, Y_{t-30}, \Delta Y_{t-6}, \dots, Y_{t-30}) + \epsilon_t, \quad (6)$$

where  $\epsilon$  is the prediction error.

Like the structural forecasting model, the nowcasting model is trained on TCs from 2000-2012, here by minimizing the mean squared error. The model is trained on data with a 2-hour resolution (rather than synoptic times alone), with intensities linearly interpolated to those times. We achieve a nowcasting RMSE/MAE of 3.4/2.4 kt on the test TCs (2013-2020); we do not include non-synoptic times in the test set. The details of the CNN architecture are given in Figure 4.

#### d. From Nowcasting to Forecasting

Section 3c defines a nowcasting model for predicting intensity at time  $t$  using the observed intensities at times  $\leq t-6$  hours and the structural trajectory at times  $\leq t$ . To predict intensity at time  $t+6$  hours, we need the intensities at times  $\leq t$  (observed, drawn from B-decks in this work) and structural trajectories at times  $\leq t+6$  hr (only observed at times  $\leq t$ ). Using the structural forecasting

model in Section 3b, we simulate many possible trajectories from times  $t+2$  hr to  $t+6$  hr. Each of these possible future trajectories is then passed to the nowcasting model to obtain a separate intensity forecast, giving an ensemble of intensity estimates.

Our proposed framework for intensity guidance has two primary benefits: (i) by providing a structural forecast, we provide insight into the TC evolution predicted by the model, such as deepening convection or the emergence of an eye in IR; (ii) because the structural forecast is stochastic, we can straightforwardly assess the uncertainty in structural evolution over time and the associated uncertainty in the intensity guidance.

## 4. Model Results

We first demonstrate the performance of our proposed model on specific cases (Hurricanes Jose [2017], Nicole [2016], and Dorian [2019]) in Section a, discussing both accuracy and the insight provided by structural forecasts at 6- and 12-hour lead times. We then assess the performance of the model during 2013-2020 in the North Atlantic basin at 6- and 12-hour lead times in Section b.

### a. Case Studies

We examine Hurricane Jose (2017) due to the presence of high vertical wind shear which produces convective asymmetries not captured by the single-profile approach (i.e., not quadrant-based) of McNeely et al. (2022). Hurricane Nicole (2016) was selected due to undergoing two rapid intensification and two rapid weakening events. Finally, Hurricane Dorian (2019) was a powerful TC with many *in situ* observations.

(i) *Intensities* Figure 5 shows the 6-hour forecasts based on 64 simulated structural trajectories per synoptic time.

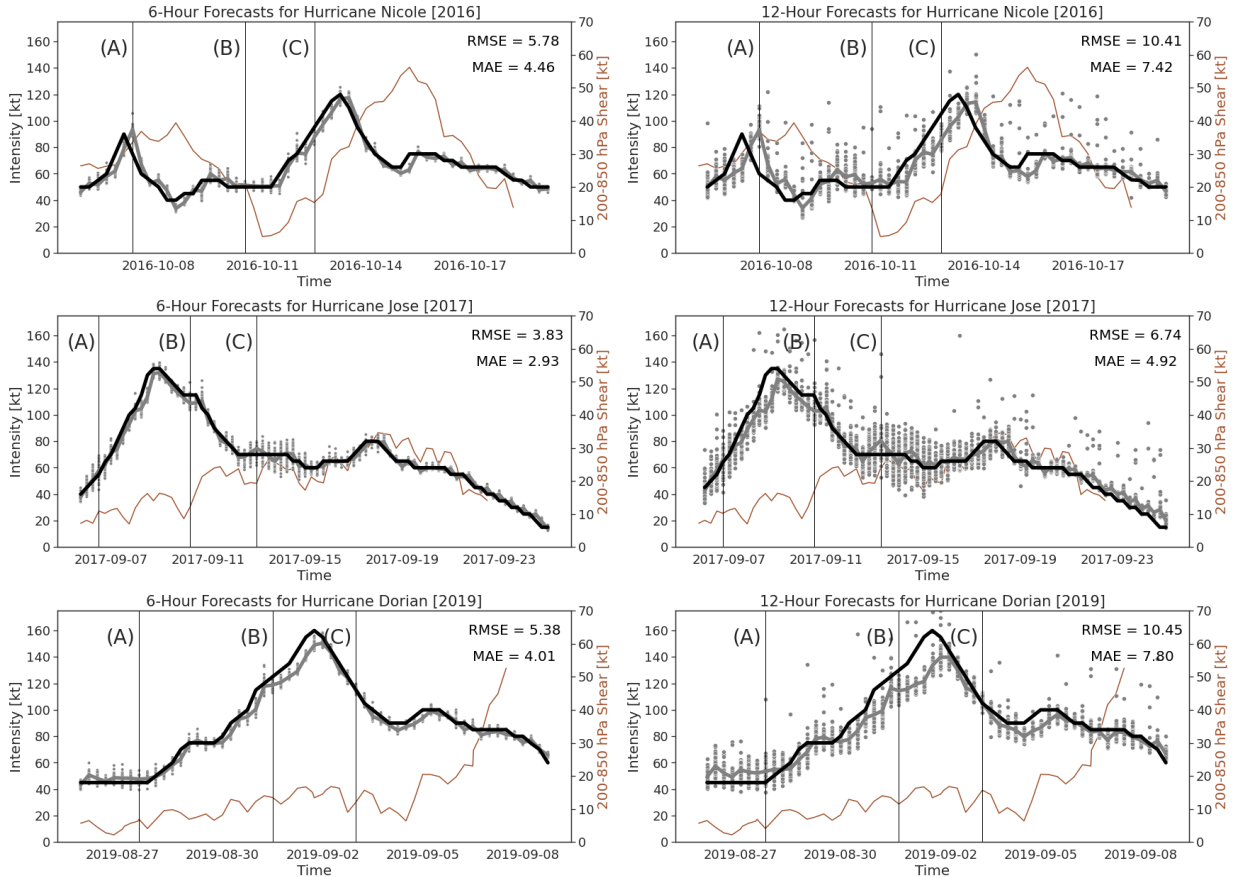


Fig. 5. **Case Studies:** Comparison of the 6-hour (left) and 12-hour (right) intensity forecasts (gray) from the structural forecasting model versus observed intensities (black). Vertical wind shear also shown (gold). The solid gray lines indicate the mean of 64 simulations at each time point. Reported errors indicate the error of the average model prediction, not individual simulations. The model captures the behavior of Hurricanes Jose [2017; center] and Dorian [2019; bottom] fairly well, but struggles with both rapid weakening events exhibited by Hurricane Nicole [2016; top] as well as low-intensity maintenance periods in Hurricanes Nicole and Dorian.

Because the structural forecasts are currently based entirely on persistence—no environmental fields, such as 200-850-hPa vertical wind shear, have been included—we expect the guidance to be most useful in the short term (6- to 12-hour time frame). The steadier development of Hurricanes Jose and Dorian are well-modeled, but the swift intensity changes exhibited by Hurricane Nicole prove challenging to capture.

Extending lead time to 12 hours increases the variation among individual simulations, but the average simulated intensity continues to roughly track the observed intensities. The rapid intensity change events exhibited by Hurricane Nicole are challenging to forecast with only IR persistence. However, the model follows Hurricane Jose’s evolution relatively well, indicating that the model has value as-is at 12-hour lead times. Still, it is clear that autoregression alone is insufficient to model the evolution of IR features; impacts of environmental characteristics such as vertical wind shear and sea surface temperatures

will be necessary to capture structural evolution beyond 12 hours.

(ii) *Diagnostics* While the end goal of intensity guidance models is ultimately prediction of TC intensity, the structural forecasting pipeline provides valuable diagnostic insight into factors contributing to its predictions. Our models (structural forecast and nowcast) should be viewed as persistence-only prototypes, as they appear to capture TC behavior well enough to demonstrate the value of stochastic structural forecasts.

Figure 6 demonstrates the 3-step (12-hour lead time) structural forecast for Hurricane Dorian out to 18 UTC 27 August during a period in which it maintained 45-kt intensity. The final 6 rows of each Hovmöller diagram are simulated from the structural forecast model; in this figure, we average the 4 quadrants for ease of visualization. Cloud-top temperature magnitude tends to be underestimated, but the expansion of cloud coverage is captured across most simulations.

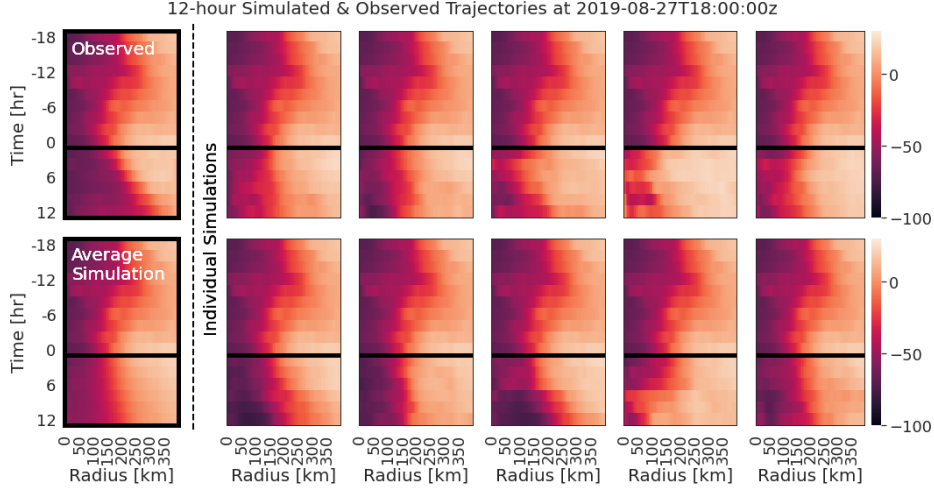


FIG. 6. **Observed and Simulated Trajectories, Hurricane Dorian [2019]:** The *observed* structural trajectory is shown in the top left corner. To the right, we see 10 *individual simulations* of radial profiles (averaged over all quadrants) at 12-hour lead times. All radial profiles above the black horizontal line are observed, while profiles below the black line are simulated. The bottom left corner shows the *arithmetic mean* over 64 simulated trajectories.

Figure 7 demonstrates the 6-hour forecasting guidance available at individual synoptic times. The average simulated profiles in each quadrant tend to track observed profiles reasonably well, although frequently predict too flat a curve and too symmetric an eye. Figure 8 is the same at the 12-hour lead time. Here, model biases tend to be amplified by longer lead times. We note that the emergence of an eye *is* captured in trajectory (B), even at the 12-hour forecast time.

Similar figures for Hurricanes Jose and Nicole are provided in the supplemental material. In general, the structural forecast follows the observed profile, even at 12-hour lead times. We did not perform any data augmentation during training (e.g., rotation) in order to preserve dominant geographic patterns (e.g., the prevalence of TC convection sheared eastward and northeastward in the North Atlantic), but it is possible that augmentation by rotating TCs would improve simulation fidelity, as it has been shown to improve accuracy in other TC intensity forecasting applications such as Griffin et al. (2022).

### b. Model Validation

The same models are used to produce 16 simulated trajectories with associated intensity guidance for each synoptic time from 2013-2020 at the 6- and 12-hour lead times. (We use 16 rather than 64 simulations when validating over the entire 8-year period for computational reasons.) Intensity predictions provided via averaging the 16 simulations are validated against HURDAT2 best-track intensities, and persistence features provided as input to the model come from operational best-tracks (“B-decks”) to emulate real-time performance.

Table 1 (left) reports validation for the simulated trajectories versus forecast lead time via root mean variance (RMV), mean absolute deviation (MAD), and bias averaged over all quadrants and radii. Let  $\bar{T}_{qi}(r)$  denote the  $i^{\text{th}}$  simulated profile in quadrant  $q$  and  $\tau_q(r)$  denote the average simulated profile in quadrant  $q$ . Then,

$$\text{RMV} = \left( \frac{1}{400 \text{ km}} \int_0^{400} \frac{1}{4n} \sum_{q=1}^4 \sum_{i=1}^n (\bar{T}_{qi}(r) - \tau_q(r))^2 dr \right)^{\frac{1}{2}}, \quad (7)$$

$$\text{MAD} = \frac{1}{400 \text{ km}} \int_0^{400} \frac{1}{4n} \sum_{q=1}^4 \sum_{i=1}^n |\bar{T}_{qi}(r) - \tau_q(r)| dr, \quad (8)$$

$$\text{Bias} = \frac{1}{400 \text{ km}} \int_0^{400} \frac{1}{4n} \sum_{q=1}^4 \sum_{i=1}^n \bar{T}_{qi}(r) - \tau_q(r) dr. \quad (9)$$

The above are defined for simulations at a single simulation time; to combine over multiple simulation times, we average MAD and bias, and average RMV in quadrature. The measures of noise (RMV and MAD) are large even for the shortest forecast lead times; increasing the simulation size beyond 16 will reduce the impact of this noise on the average forecast. Bias, meanwhile, becomes steadily more negative with time. This will lead to overestimates of intensity, as low IR temperatures are generally associated with stronger TCs.

Table 1(right) reports validation for intensity guidance using the traditional definitions for root mean squared error (RMSE), mean absolute error (MAE), and bias. As expected, the negative bias in structural forecasts manifests as a positive bias in intensity guidance.

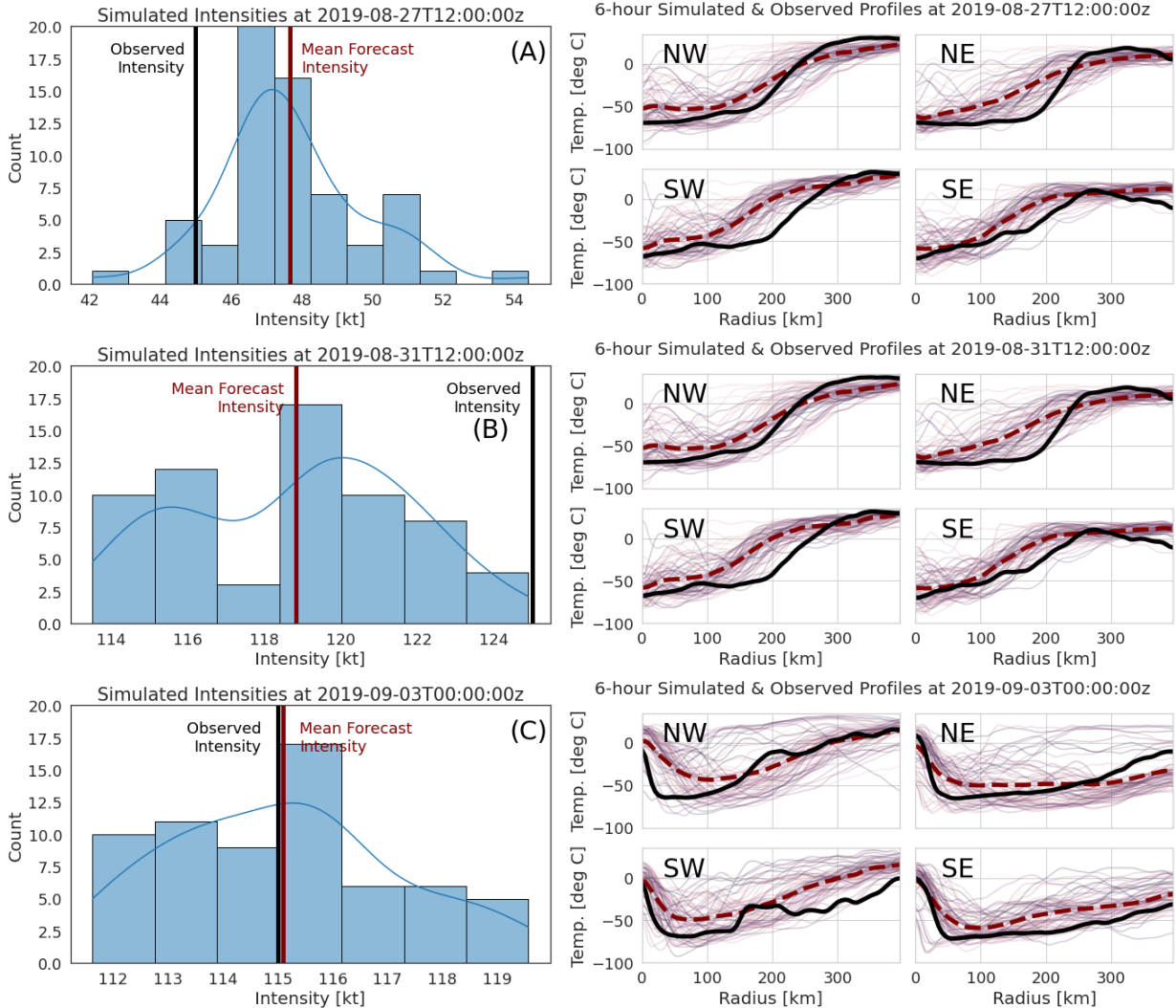


FIG. 7. **Hurricane Dorian [2019] 6-hr Guidance:** (Left) Distribution of forecasted intensities with observed (black) and average forecast (red) intensities marked. (Right) Simulated profiles by quadrant with observed profiles represented by solid black curves, and averaged simulated profiles represented by dashed red curves.

Tables 2 and 3 assess the performance of our intensity guidance via structural forecasting at 12-hour lead times and compare it to the NHC's official forecast validation from 2013-2019 due to availability of validation data at time of writing; note that this is a subset of the times reported in Table 1. Overall, the RMSE of the structural forecast is about 1.3 kt larger than the NHC official forecast error with roughly twice the bias (1.1 kt vs -0.6 kt). The structural forecast sees unchanged MSE with increasing 200-850-hPa vertical wind shear; the bias, however, increases with increasing wind shear (Table 2). This trend is expected, as the model does not include wind shear as a predictor but instead relies on the relationship between shear and asymmetry in IR imagery (as captured by the quadrants of the radial profiles). The NHC official forecast

error exhibits a similar, if less pronounced, trend in bias with increasing shear. The direction of shear seems more important, with both our model and the NHC official forecast performing most poorly for NW shear (6% of cases) and best for SW shear (9% of cases). The NE and SE cases dominate the overall model performance. The disparity between different shear magnitudes and directions could be alleviated in a model which utilizes environmental predictors.

Table 3 demonstrates similar error trends for both official forecasts and our structural forecasts. Errors tend to increase with TC intensity and with rate of intensification or weakening. The structural model produces higher bias for weaker TCs and lower bias for stronger TCs. Similarly, the structural model tends to overestimate intensities

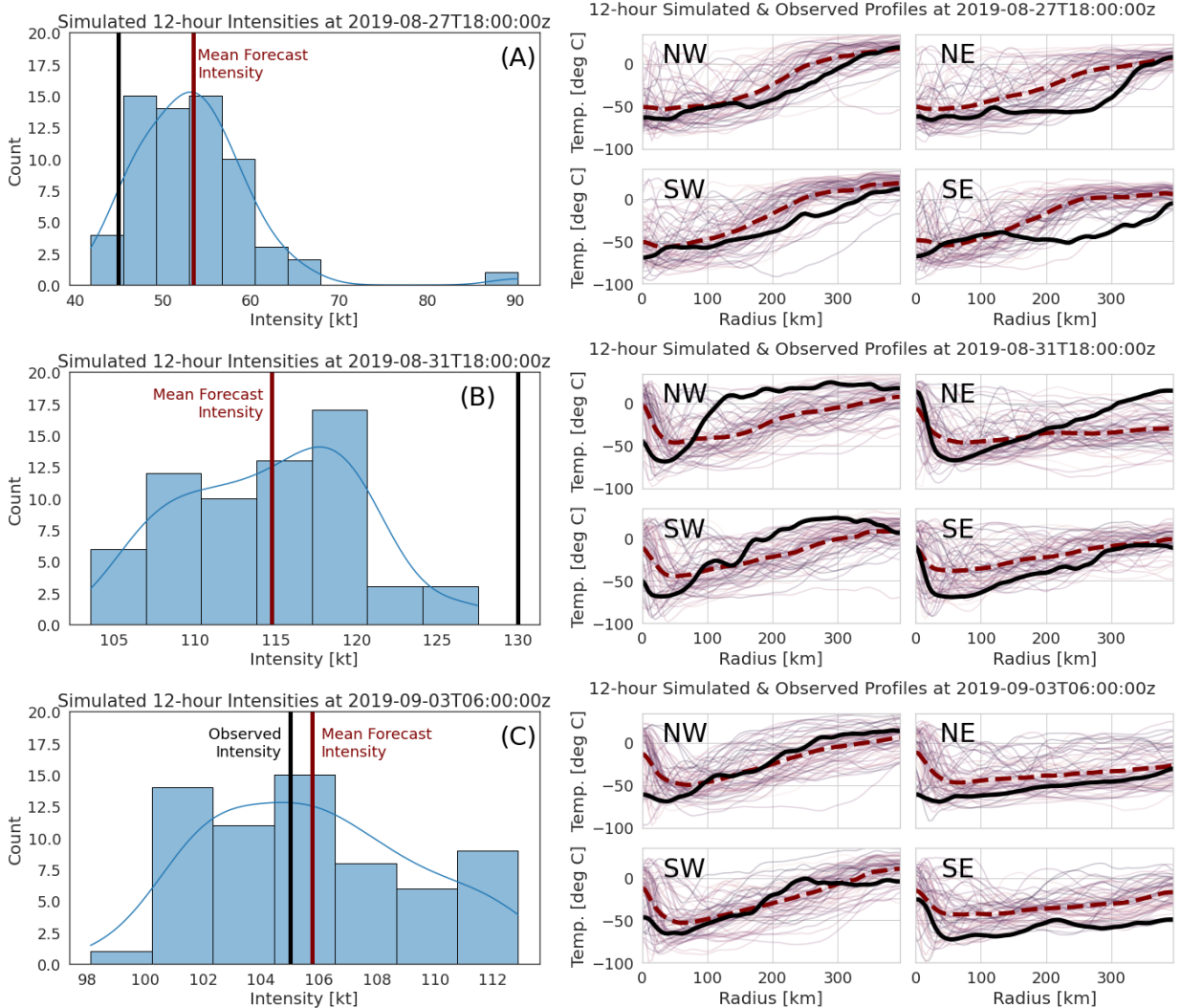


FIG. 8. **Hurricane Dorian [2019] 12-hr Guidance:** Model bias during intensification (center row) is more exaggerated at 12-hour lead times. (Left) Distribution of forecasted intensities with observed (black) and average forecast (red) intensities marked. (Right) Simulated profiles by quadrant with observed profiles represented by solid black curves, and averaged simulated profiles represented by dashed red curves.

during weakening and underestimate them during intensification. The model errors are comparable to NHC official forecast errors during periods of maintenance and intensification (although bias is higher); it is periods of weakening which tend to be poorly modeled by the structural forecast. We suspect that the inclusion of environmental information could improve fidelity in weakening cases; see the following section for a discussion of such avenues for model improvement.

## 5. Discussion and Conclusion

### a. Inclusion of Environmental Variables

The PixelSNAIL model presented here is a purely autoregressive process; that is, it simulates future structural features using only past IR imagery as an input. The inclusion of environmental variables known to impact TCs such as vertical wind shear, atmospheric moisture, or sea surface temperature may improve the accuracy of the forward simulation of radial profiles. Such factors can be added to the PixelSNAIL architecture as additional input layers via values provided by SHIPS which are not forecasted by the model. These inputs would then serve as “guidrails” for simulated structural evolution with potential to better cap-

ture the effects of such factors on profile asymmetry. Furthermore, the inclusion of current environmental variables in the nowcasting model is likely to improve its intensity estimates and enable a more direct comparison of its performance to NHC official forecasts. Despite these limitations, the model presented in this work provides reasonable intensity estimates and short-term forecasts derived solely from past TC intensity estimates, past Geo IR imagery, and predicted TC structural characteristics.

#### *b. Improving the Network Architecture for Structural Forecasts*

The PixelSNAIL approach provides reasonable simulations of TC IR structural evolution up to 12-hour lead times. However, there exists a wealth of alternate deep autoregressive generative models, each of which can be designed and trained in innumerable ways. Likewise, deep autoregressive models are not the only generative models available. Simulation could be carried out via vector autoregression on a low-dimensional projection of profiles (e.g., principal component analysis, Fourier bases, etc.), generative adversarial networks (GANs; Creswell et al. (2018)), or other approaches. The PixelSNAIL architecture is chosen to demonstrate the value and feasibility of structural forecasting for intensity guidance.

#### *c. Validating and Correcting the Probability Distribution of Structural Forecasts*

Our structural forecasts are probabilistic in nature, taking the form of probability distributions over future structural trajectories  $\mathbf{S}_{>t}$ . In the current work, we apply a standard machine learning approach of fitting a model by minimizing a loss function (in this case the negative log likelihood). A good probabilistic forecast, however, should be *conditionally calibrated*. That is, the probability of a particular event (in our case, specific radial profiles 6-12 hours into the future), given or “conditional on” a particular history of evolution and other predictors, should match the predicted probability of the same event. This is essentially saying that draws from the forecasting model should be indistinguishable from actual observations, if all relevant conditions are the same. Dey et al. (2022) recently proposed a new method for adjusting or “recalibrating” probabilistic forecasts, so that they will have this property. Indeed, one can potentially apply their procedure sequentially to each autoregressive component  $p(Z_{iq}|Z_{i-1}, \dots, Z_1)$ , for pixel  $i = 1, \dots, n$ , and quadrant  $q = 1, 2, 3, 4$ , so as to obtain a conditionally calibrated density over structural trajectories  $\mathbf{S}_{>t}$  given present and past observations; see Discussion in Dey et al. (2022).

#### *d. Conclusion*

This paper demonstrates a novel approach to short-term TC intensity guidance solely using past TC intensity estimates and past and current IR observations. By predicting TC IR structure through radial profiles computed over four geographic quadrants, we obtain reasonable estimates of future TC intensity while simultaneously capturing *signals* in convective structure relevant to those future intensities. We also focus on interpretable, physically-based factors to facilitate understanding of the model’s performance (e.g., upcoming intensification corresponds with decreasing cloud-top temperatures in the structural forecast). The approach outlined here has the potential for further refinement by including environmental predictors provided in real time by SHIPS guidance. Though testing on years of cases takes time, an individual forecast for a single TC can be obtained in minutes on a single GPU, indicating the potential for the eventual use of this model as part of the available TC guidance suite in an operational setting.

*Acknowledgments.* Parts of this research were done while Pavel Khokhlov was a student at Carnegie Mellon University. The authors are grateful to Galen Vincent for many discussions and helpful comments on the research. This work is supported in part by NSF DMS-2053804, NSF PHY-2020295, and the C3.ai Digital Transformation Institute.

*Data availability statement.* Code to generate Geo IR radial profiles from openly available data can be found at <https://github.com/ihmcneely/ORB2sample>, which draws from the MERGIR database openly available from NASA at [https://disc.gsfc.nasa.gov/datasets/GPM\\_MERGIR\\_1/summary](https://disc.gsfc.nasa.gov/datasets/GPM_MERGIR_1/summary). The HURDAT2 best track database is openly available from the NHC at <https://www.nhc.noaa.gov/data>, while the ATCF operational best tracks (B-deck) are openly available from the National Center for Atmospheric Research at <http://hurricanes.ral.ucar.edu/repository/>. Official forecast validation files are openly available from the NHC at <https://www.nhc.noaa.gov/verification/>. Finally, SHIPS developmental data is openly available from the Cooperative Institute for Research in the Atmosphere at [https://rammb.cira.colostate.edu/research/tropical\\_cyclones/ships/developmental\\_data.asp](https://rammb.cira.colostate.edu/research/tropical_cyclones/ships/developmental_data.asp).

Trajectory Validation							Intensity Validation		
Lead time	2 h	4 h	6 h	8 h	10 h	12 h	Lead time	6 h	12 h
RMV	10.5C	14.7C	17.4C	22.2C	25.1C	26.9C	RMSE	4.9 kt	9.5 kt
MAD	7.1C	10.5C	12.8C	15.6C	17.6C	19.0C	MAE	3.4 kt	7.1 kt
Bias	-0.6C	-2.2C	-4.0C	-6.3C	-7.9C	-9.3C	Bias	0.7 kt	2.8 kt

TABLE 1. **Overall Model Validation at n = 16:** (Left) Structure validation versus observed profiles. Simulation noise (root mean variance and mean absolute deviation) grows rapidly in the first 6 hours; bias increases in magnitude steadily. (Right) Intensity validation vs HURDAT2 best-track intensities from 2013-2020 at each lead time.

Shear Magnitude				Shear Direction			
Shear	Structural	NHC OFCL	N	Shear Direction	Structural	NHC OFCL	N
	12-h RMSE/MAE/Bias				12-h RMSE/MAE/Bias		
0-10 kt	9.3/7.2/-0.7 kt	9.3/6.3/-1.1 kt	246	SW	8.6/6.1/0.0 kt	7.4/5.4/-1.0 kt	108
10-20 kt	9.7/6.9/1.1 kt	8.1/5.6/-0.5 kt	513	SE	9.1/7.0/0.3 kt	8.5/5.9/-0.6 kt	444
20+ kt	9.0/6.5/2.2 kt	7.5/5.1/-0.6 kt	449	NE	9.5/6.7/2.4 kt	7.8/5.3/-0.6 kt	586
				NW	10.7/8.2/-2.0 kt	8.9/6.1/-0.9 kt	70
Total	9.4/6.8/1.1 kt	8.1/5.6/-0.6 kt	1,208	Total	9.4/6.8/1.1 kt	8.1/5.6/-0.6 kt	1,208

TABLE 2. **Intensity Guidance Validation Relative to Shear:** Model validation binned by 200-850-hPa vertical wind shear, reported as RMSE/MAE/Bias. (Left) The performance of the structural forecasting model does not change meaningfully relative to wind shear magnitude, while the NHC official forecast performs better in higher shear environments. The structural forecast has comparable performance to the NHC official forecasts in low-shear environments. (Right) The performance of the structural model does vary with shear direction. Both the NHC forecasts and the structural model produce higher errors for NW shear (6% of cases).

TC Intensity				Intensity Change			
Category	Structural	NHC OFCL	N	Evolution	Structural	NHC OFCL	N
	12-h RMSE/MAE/Bias				12-h RMSE/MAE/Bias		
Tropical Depression	5.5/4.4/3.0 kt	5.9/4.2/-2.9 kt	114	Weakening	12.0/8.9/7.6 kt	7.8/5.4/2.8 kt	266
Tropical Storm	7.3/5.7/2.8 kt	6.3/4.4/-0.7 kt	578	Maintenance	6.7/5.3/3.4 kt	6.0/4.3/0.0 kt	506
Hurricane	10.3/7.7/0.7 kt	9.2/6.7/-0.5 kt	357	Intensifying	10.2/7.4/-5.4 kt	10.2/7.1/-3.5 kt	436
Major Hurricane	14.6/10.9/-5.1 kt	11.7/8.3/0.9 kt	159	Total	9.4/6.8/1.1 kt	8.1/5.6/-0.6 kt	1,208
Total	9.4/6.8/1.1 kt	8.1/5.6/-0.6 kt	1,208				

TABLE 3. **Intensity Guidance Validation by TC Intensity:** Model validation split out by intensity and intensity change, reported as RMSE/MAE/Bias. (Left) Both the structural and NHC official forecasts struggle more with intense storms, which are rarer. The structural forecast has much stronger bias, which is expected due to the heavy influence of persistence features in the absence of environmental predictors. (Right) Similarly, both forecasts perform best during maintenance periods (6-hour change  $\leq 5$  kt in magnitude), overestimate during weakening, and underestimate during intensification. The bias is more pronounced in the structural forecast due to the absence of environmental predictors.

## References

- Chen, X., N. Mishra, M. Rohaninejad, and P. Abbeel, 2018: Pixelsnail: An improved autoregressive generative model. *International Conference on Machine Learning*, PMLR, 864–872.
- Combinido, J. S., J. R. Mendoza, and J. Aborot, 2018: A convolutional neural network approach for estimating tropical cyclone intensity using satellite-based infrared images. *2018 24th International Conference on Pattern Recognition (ICPR)*, IEEE, 1474–1480.
- Creswell, A., T. White, V. Dumoulin, K. Arulkumaran, B. Sengupta, and A. A. Bharath, 2018: Generative adversarial networks: An overview. *IEEE Signal Processing Magazine*, **35** (1), 53–65.
- DeMaria, M., 2018: SHIPS developmental database file format and predictor descriptions (2018). Tech. rep., Colorado State University. URL [http://rammb.cira.colostate.edu/research/tropical\\_cyclones/ships/docs/ships\\_predictor\\_file\\_2018.doc](http://rammb.cira.colostate.edu/research/tropical_cyclones/ships/docs/ships_predictor_file_2018.doc), Developmental Data.
- DeMaria, M., and J. Kaplan, 1999: An updated statistical hurricane intensity prediction scheme (SHIPS) for the Atlantic and Eastern North Pacific basins. *Weather and Forecasting*, **14** (3), 326–337.
- DeMaria, R., 2015: Automated tropical cyclone eye detection using discriminant analysis. Ph.D. thesis, Colorado State University.
- Dey, B., D. Zhao, J. A. Newman, B. H. Andrews, R. Izbicki, and A. B. Lee, 2022: Calibrated predictive distributions via diagnostics for conditional coverage. *arXiv preprint arXiv:2205.14568*.
- Dvorak, V. F., 1975: Tropical cyclone intensity analysis and forecasting from satellite imagery. *Monthly Weather Review*, **103** (5), 420–430, [https://doi.org/10.1175/1520-0493\(1975\)103<0420:TCIAAF>2.0.CO;2](https://doi.org/10.1175/1520-0493(1975)103<0420:TCIAAF>2.0.CO;2).
- Ebert-Uphoff, I., and K. Hilburn, 2020: Evaluation, tuning, and interpretation of neural networks for working with images in meteorological applications. *Bulletin of the American Meteorological Society*, **101** (12), E2149–E2170.
- Gray, W. M., 1979: Hurricanes: Their formation, structure and likely role in the tropical circulation. *Meteorology over the tropical oceans*, **155**, 218.
- Griffin, S. M., A. Wimmers, and C. S. Velden, 2022: Predicting rapid intensification in north atlantic and eastern north pacific tropical cyclones using a convolutional neural network. *Weather and Forecasting*.
- Hovmöller, E., 1949: The trough-and-ridge diagram. *Tellus*, **1** (2), 62–66.
- Hu, L., E. A. Ritchie, and J. S. Tyo, 2020: Short-term tropical cyclone intensity forecasting from satellite imagery based on the deviation angle variance technique. *Weather and Forecasting*, **35** (1), 285–298.
- Janowiak, J., B. Joyce, and P. Xie, 2020: NCEP/CPC L3 half hourly 4km global (60S - 60N) merged IR v1. NASA Goddard Earth Sciences Data and Information Services Center, URL [https://disc.gsfc.nasa.gov/datacollection/GPM\\_MERGIR\\_1.html](https://disc.gsfc.nasa.gov/datacollection/GPM_MERGIR_1.html), <https://doi.org/10.5067/P4HZB9N27EKU>.
- Knaff, J. A., and R. T. DeMaria, 2017: Forecasting tropical cyclone eye formation and dissipation in infrared imagery. *Weather and Forecasting*, **32** (6), 2103–2116.
- Knapp, K. R., and S. L. Wilkins, 2018: Gridded satellite (GridSat) GOES and CONUS data. *Earth System Science Data*, **10** (3), 1417–1425, <https://doi.org/10.5194/essd-10-1417-2018>.
- Landsea, C. W., and J. L. Franklin, 2013: Atlantic hurricane database uncertainty and presentation of a new database format. *Monthly Weather Review*, **141** (10), 3576–3592, <https://doi.org/10.1175/MWR-D-12-00254.1>.
- Lee, J., J. Im, D.-H. Cha, H. Park, and S. Sim, 2019: Tropical cyclone intensity estimation using multi-dimensional convolutional neural networks from geostationary satellite data. *Remote Sensing*, **12** (1), 108.
- Liu, Z., 2021: private communication.
- McGovern, A., R. Lagerquist, D. J. Gagne, G. E. Jergensen, K. L. Elmore, C. R. Homeyer, and T. Smith, 2019: Making the black box more transparent: Understanding the physical implications of machine learning. *Bulletin of the American Meteorological Society*, **100** (11), 2175–2199.
- McNeely, T., A. B. Lee, D. Hammerling, and K. Wood, 2019: Quantifying the spatial structure of tropical cyclone imagery.
- McNeely, T., A. B. Lee, K. M. Wood, and D. Hammerling, 2020: Unlocking GOES: A statistical framework for quantifying the evolution of convective structure in tropical cyclones. *Journal of Applied Meteorology and Climatology*, **59** (10), 1671–1689.
- McNeely, T., G. Vincent, A. B. Lee, R. Izbicki, and K. M. Wood, 2022: Detecting distributional differences in labeled sequence data with application to tropical cyclone satellite imagery. *arXiv preprint arXiv:2202.02253*.
- NHC, 2022: Official NHC Atlantic track and intensity forecast errors. Accessed: 2022-03-31, <https://www.nhc.noaa.gov/verification/verify7.shtml>.
- Olander, T. L., and C. S. Velden, 2007: The advanced dvorak technique: Continued development of an objective scheme to estimate tropical cyclone intensity using geostationary infrared satellite imagery. *Weather and Forecasting*, **22** (2), 287–298.

- Olander, T. L., and C. S. Velden, 2019: The advanced dvorak technique (adt) for estimating tropical cyclone intensity: Update and new capabilities. *Weather and Forecasting*, **34** (4), 905–922.
- Pradhan, R., R. S. Aygun, M. Maskey, R. Ramachandran, and D. J. Cecil, 2017: Tropical cyclone intensity estimation using a deep convolutional neural network. *IEEE Transactions on Image Processing*, **27** (2), 692–702.
- Salimans, T., A. Karpathy, X. Chen, and D. P. Kingma, 2017: Pixelcnn++: Improving the pixelcnn with discretized logistic mixture likelihood and other modifications. *arXiv preprint arXiv:1701.05517*.
- Sampson, C. R., and A. J. Schrader, 2000: The automated tropical cyclone forecasting system (version 3.2). *Bulletin of the American Meteorological Society*, **81** (6), 1231–1240.
- Sanabia, E. R., B. S. Barrett, and C. M. Fine, 2014: Relationships between tropical cyclone intensity and eyewall structure as determined by radial profiles of inner-core infrared brightness temperature. *Monthly Weather Review*, **142** (12), 4581–4599, <https://doi.org/10.1175/MWR-D-13-00336.1>.
- Schmit, T. J., P. Griffith, M. M. Gunshor, J. M. Daniels, S. J. Goodman, and W. J. Lehair, 2017: A closer look at the ABI on the GOES-R series. *Bulletin of the American Meteorological Society*, **98** (4), 681–698.
- Tian, W., W. Huang, L. Yi, L. Wu, and C. Wang, 2020: A cnn-based hybrid model for tropical cyclone intensity estimation in meteorological industry. *IEEE Access*, **8**, 59 158–59 168.
- Van den Oord, A., N. Kalchbrenner, L. Espeholt, O. Vinyals, A. Graves, and Coauthors, 2016: Conditional image generation with pixelcnn decoders. *Advances in neural information processing systems*, **29**.
- Van Oord, A., N. Kalchbrenner, and K. Kavukcuoglu, 2016: Pixel recurrent neural networks. *International conference on machine learning*, PMLR, 1747–1756.
- Wang, C., Q. Xu, X. Li, and Y. Cheng, 2020: Cnn-based tropical cyclone track forecasting from satellite infrared images. *IGARSS 2020-2020 IEEE International Geoscience and Remote Sensing Symposium*, IEEE, 5811–5814.
- Zhang, C.-J., X.-J. Wang, L.-M. Ma, and X.-Q. Lu, 2021: Tropical cyclone intensity classification and estimation using infrared satellite images with deep learning. *IEEE Journal of Selected Topics in Applied Earth Observations and Remote Sensing*, **14**, 2070–2086.

## Supplemental Materials

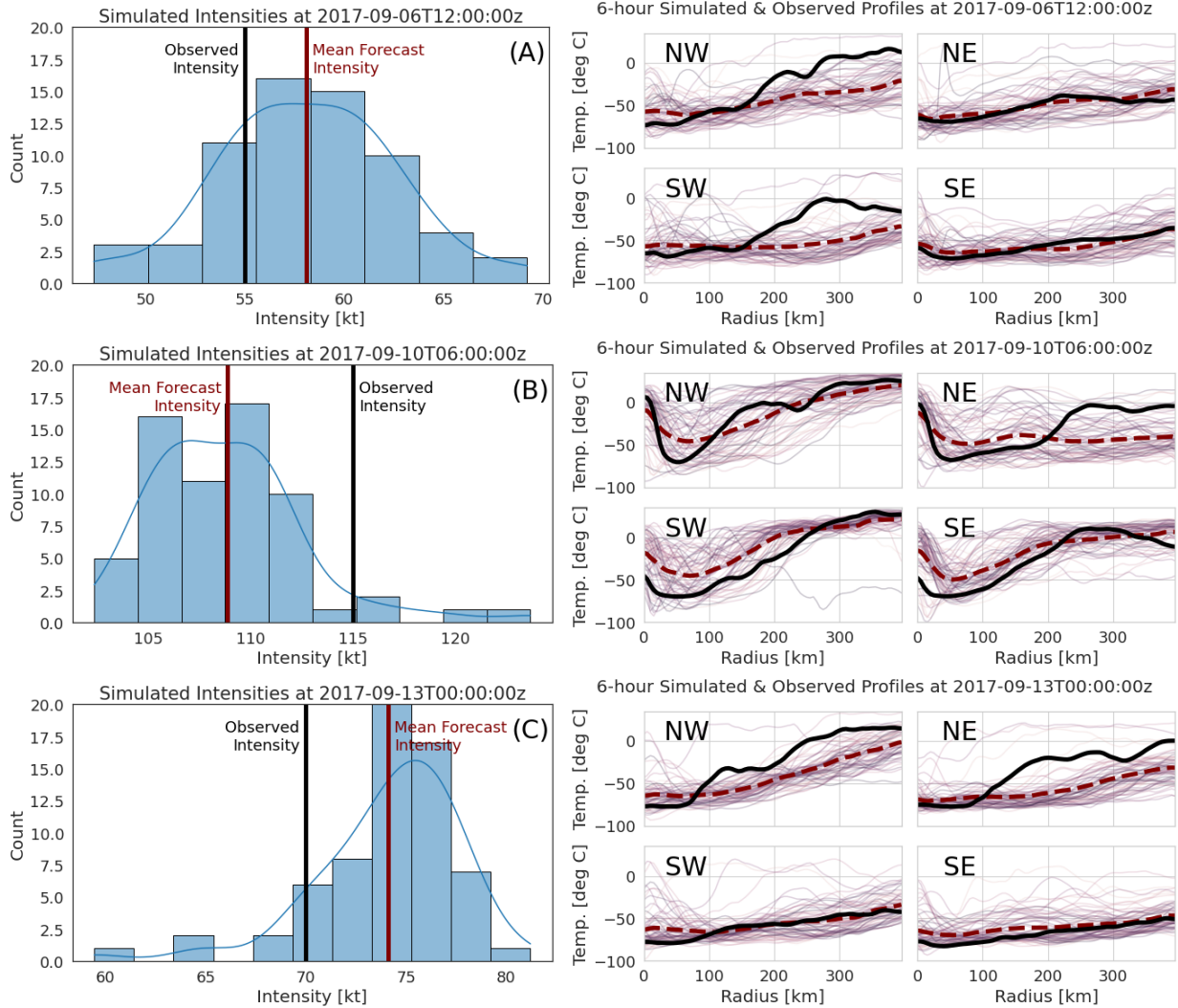


FIG. 9. **Hurricane Jose [2017] 6-hr Guidance:** Hurricane Jose was subjected to vertical wind shear out of the west/northwest due to Hurricane Irma; the structural forecasts tend to underestimate temperatures in the NW quadrant and thus overestimate TC intensity. (Left) Distribution of forecasted intensities with observed (black) and average forecast (red) intensities marked. (Right) Simulated profiles by quadrant with observed profiles represented by solid black curves, and averaged simulated profiles represented by dashed red curves.

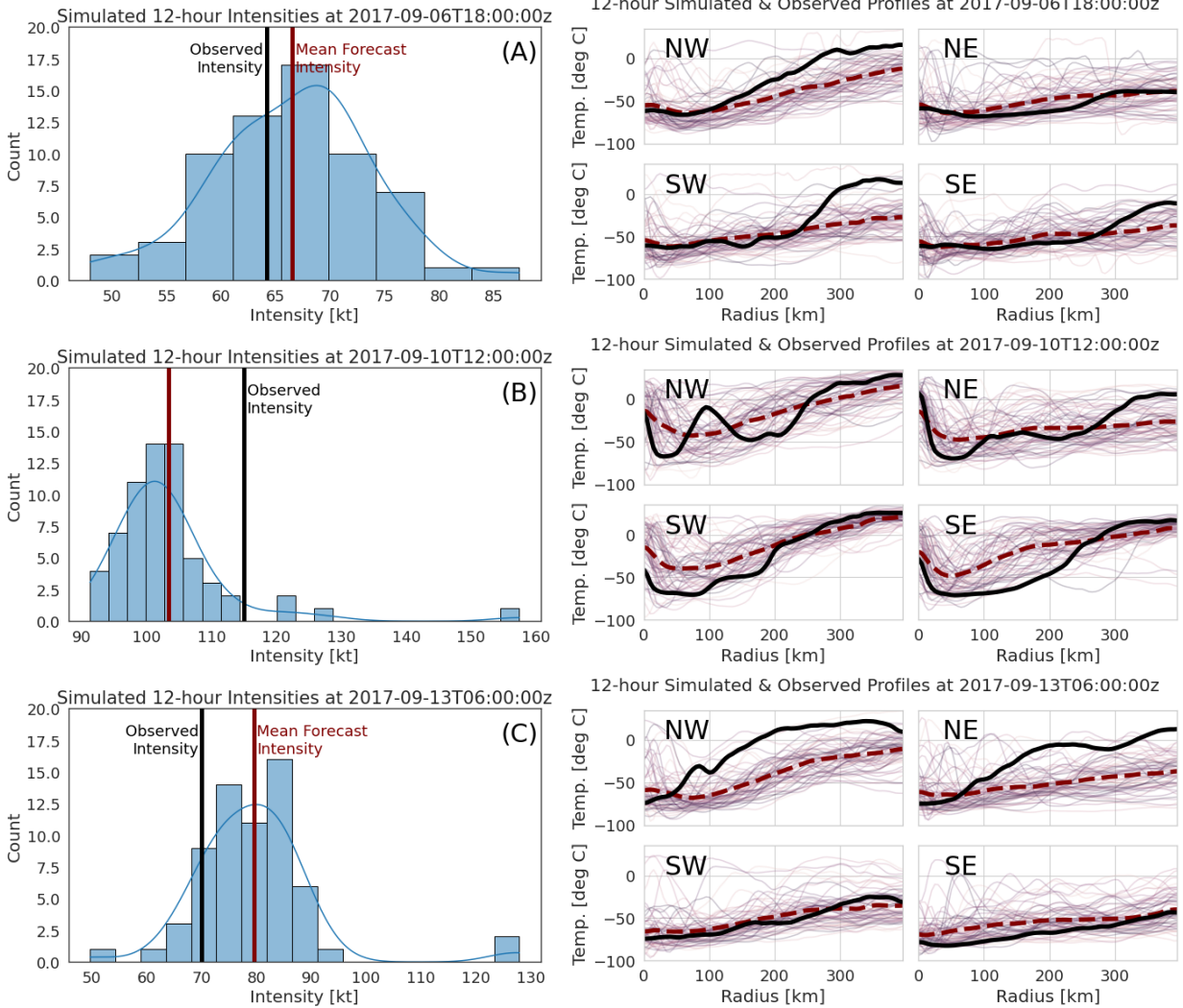


FIG. 10. **Hurricane Jose [2017] 12-hr Guidance:** At 12-hour lead times, this TC's evolution is still well modeled save for a handful of individual overestimates. (Left) Distribution of forecasted intensities with observed (black) and average forecast (red) intensities marked. (Right) Simulated profiles by quadrant with observed profiles represented by solid black curves, and averaged simulated profiles represented by dashed red curves.

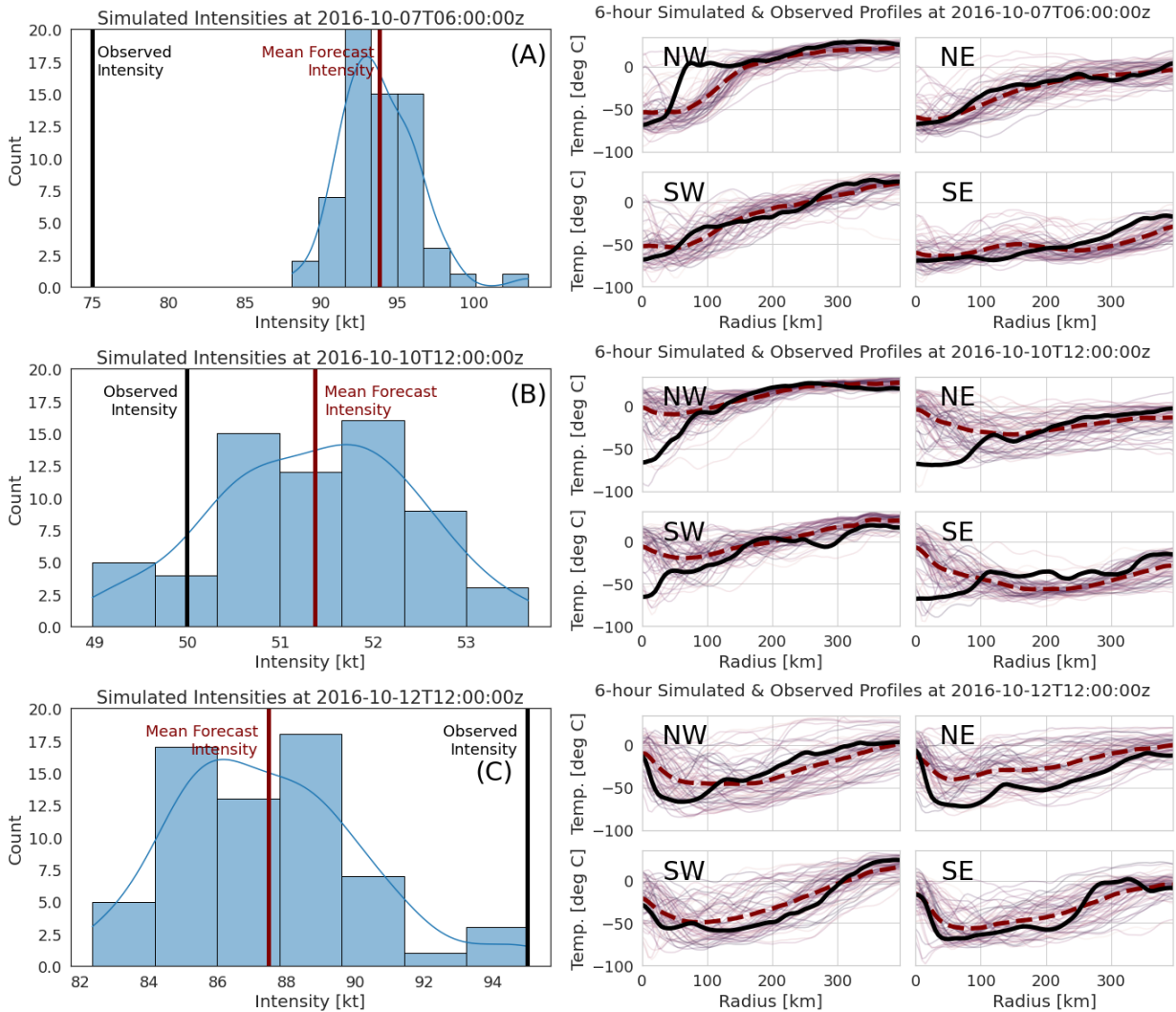


FIG. 11. **Hurricane Nicole [2016] 6-hr Guidance:** Hurricane Nicole underwent several rapid intensity change events. At 6 UTC 7 October, the structural forecast models the cloud top temperatures well, but this is insufficient to predict the extreme change from intensification to weakening even at 6-hour lead times. (Left) Distribution of forecasted intensities with observed (black) and average forecast (red) intensities marked. (Right) Simulated profiles by quadrant with observed profiles represented by solid black curves, and averaged simulated profiles represented by dashed red curves.

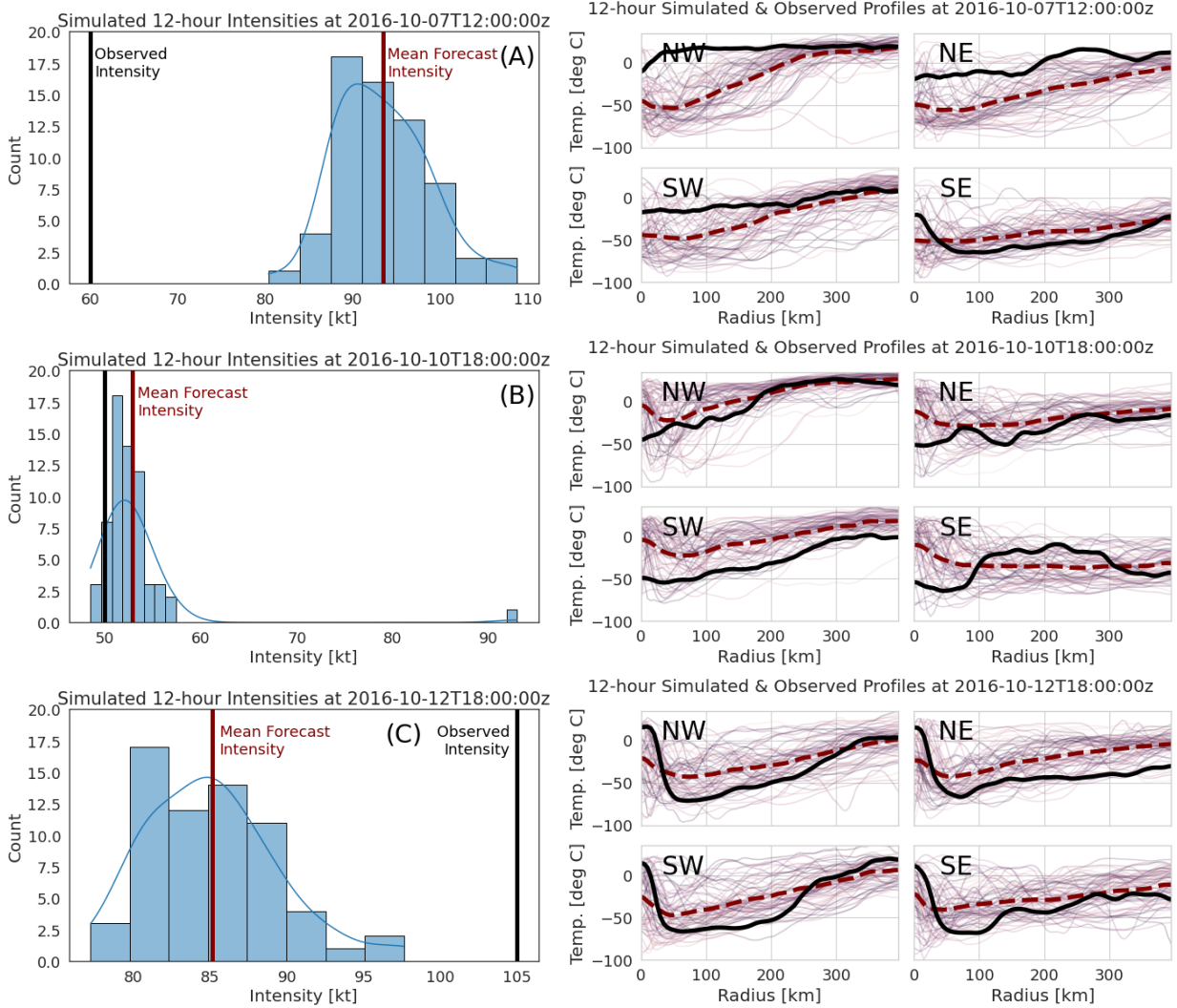


FIG. 12. **Hurricane Nicole [2016] 12-hr Guidance:** Model biases during the quick shifts from intensification to weakening and during steady intensification are exacerbated at 12-hour lead times. (Left) Distribution of forecasted intensities with observed (black) and average forecast (red) intensities marked. (Right) Simulated profiles by quadrant with observed profiles represented by solid black curves, and averaged simulated profiles represented by dashed red curves.

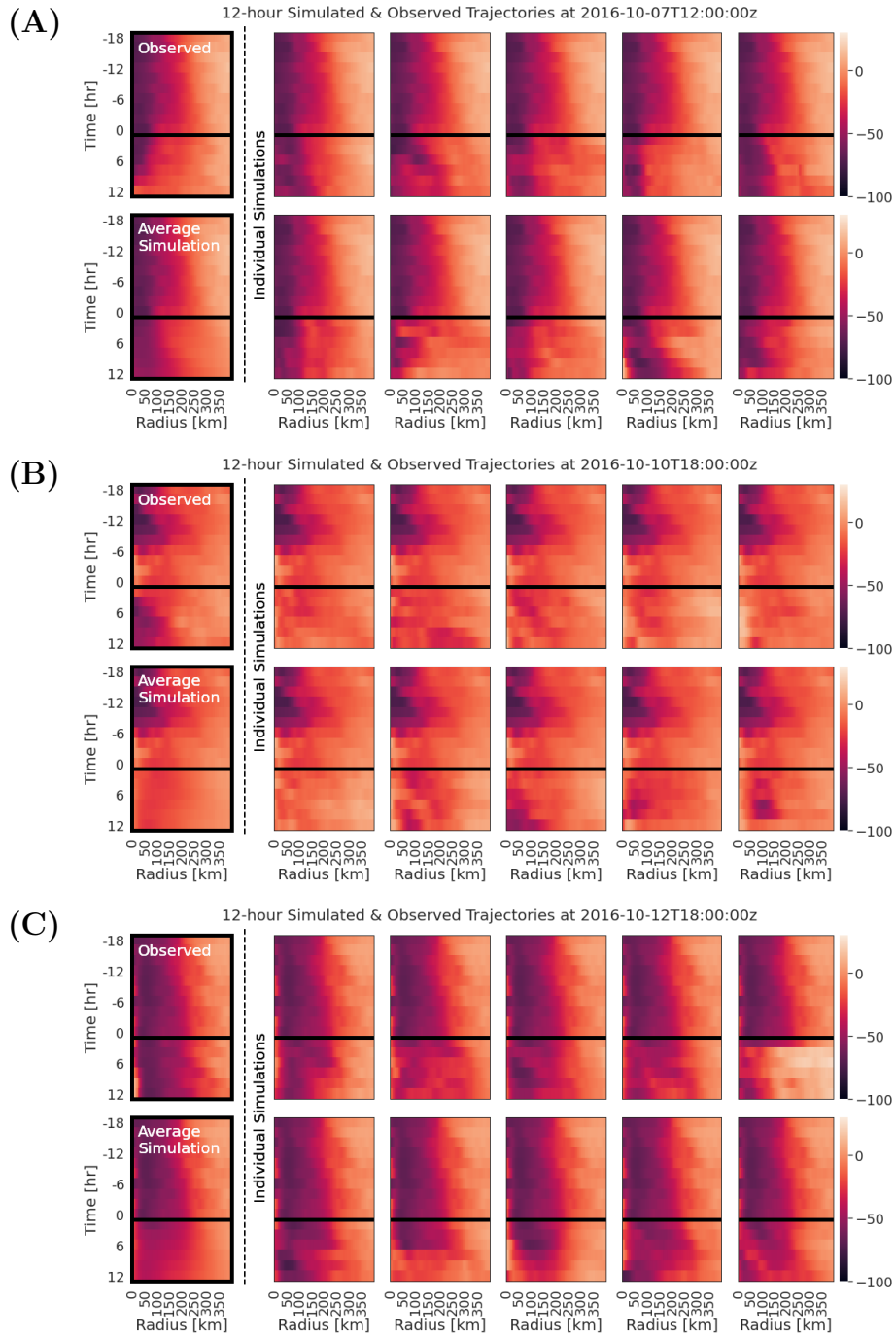


FIG. 13. **Hurricane Nicole [2016] 12-hr Structural Forecasts:** The *observed* structural trajectory is shown in the top left corner of each row. To the right, we see 10 *individual simulations* of radial profiles (averaged over all quadrants) at 12-hour lead times. All radial profiles above the black horizontal line are observed, while profiles below the black line are simulated. The bottom left corner, shows the *average simulation* over 64 simulated trajectories.

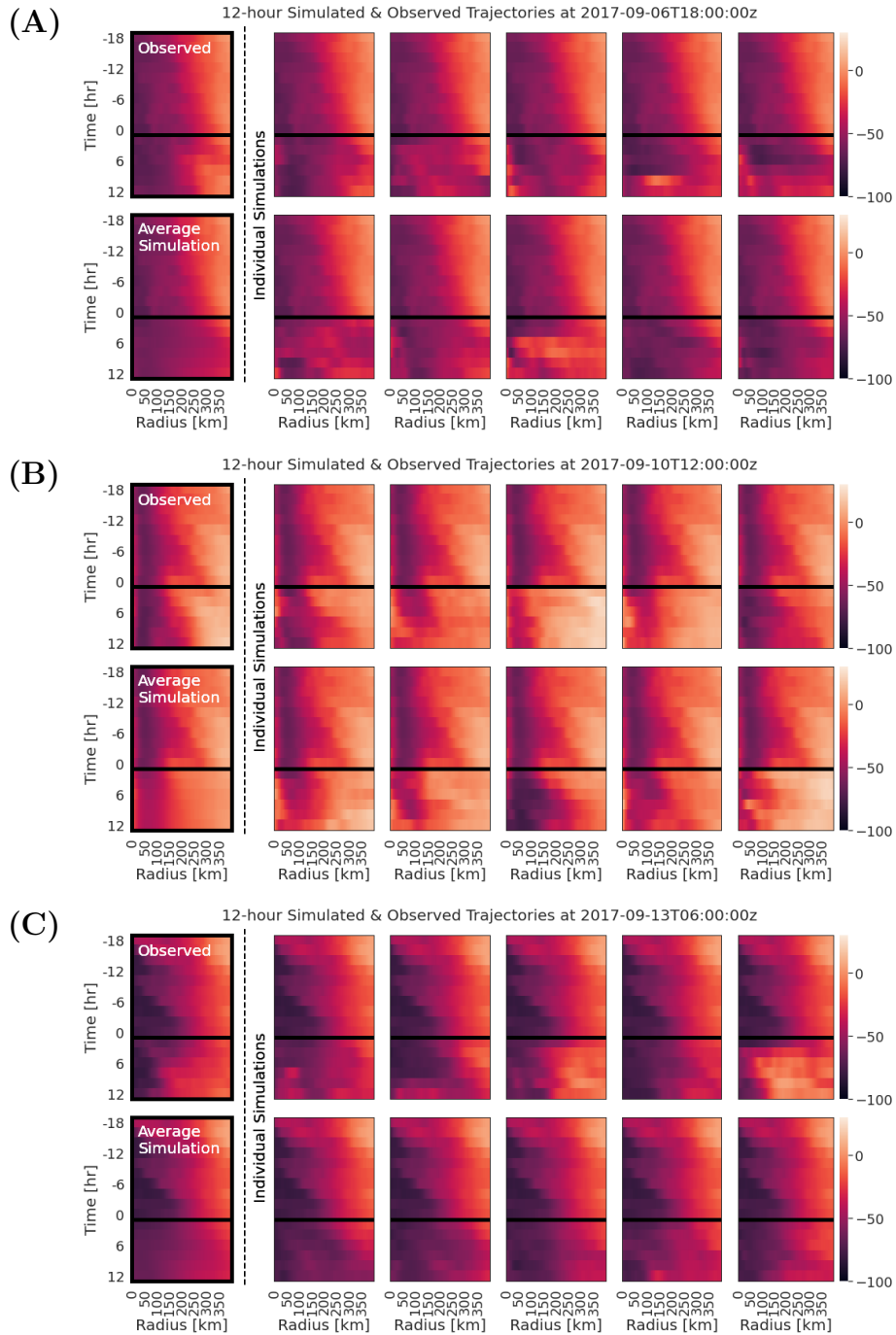


FIG. 14. **Hurricane Jose [2017] 12-hr Structural Forecasts:** The *observed* structural trajectory is shown in the top left corner of each row. To the right, we see 10 *individual simulations* of radial profiles (averaged over all quadrants) at 12-hour lead times. All radial profiles above the black horizontal line are observed, while profiles below the black line are simulated. The bottom left corner, shows the *average simulation* over 64 simulated trajectories.

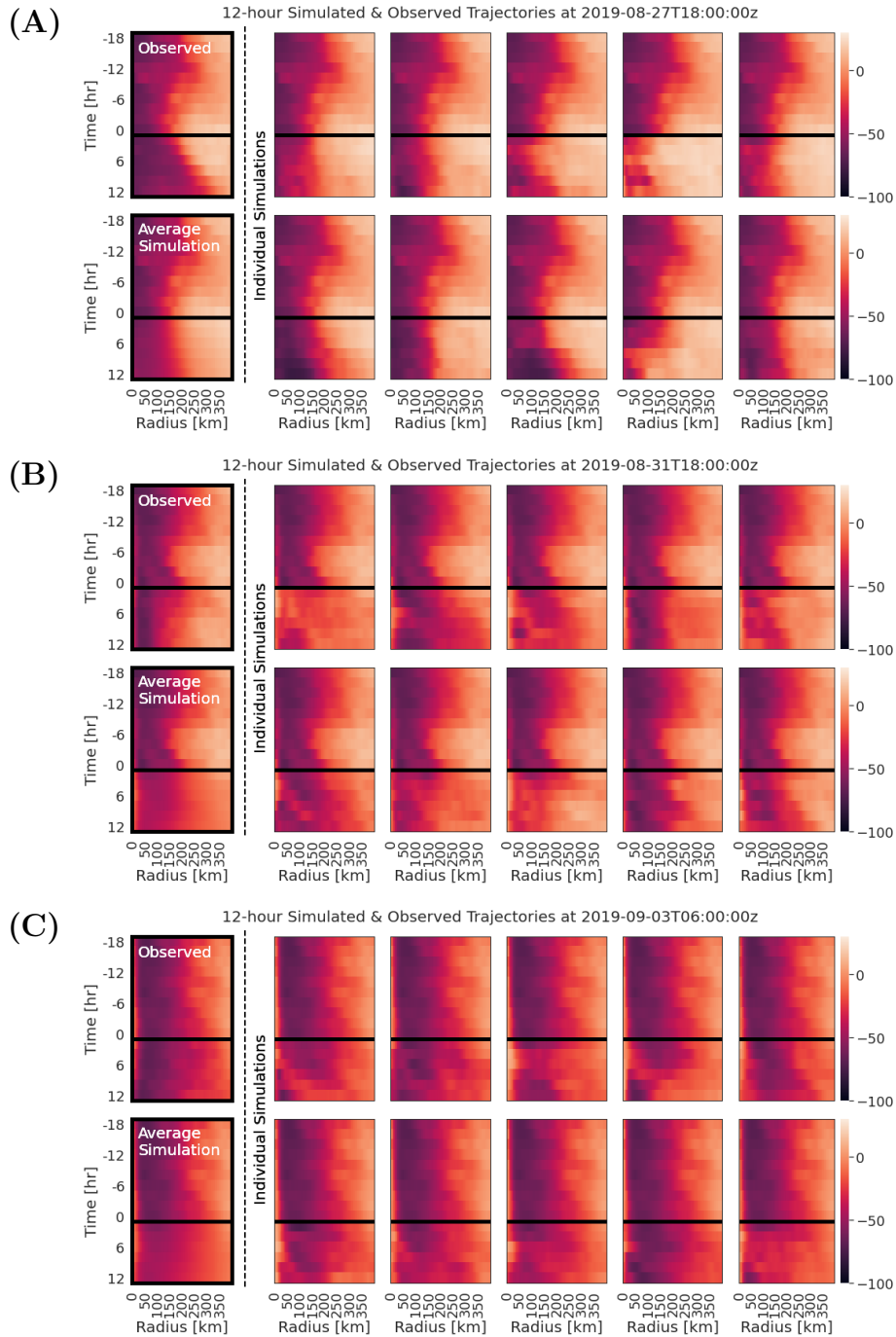


FIG. 15. **Hurricane Dorian (2019) 12-hr Structural Forecasts:** The *observed* structural trajectory is shown in the top left corner of each row. To the right, we see 10 *individual simulations* of radial profiles (averaged over all quadrants) at 12-hour lead times. All radial profiles above the black horizontal line are observed, while profiles below the black line are simulated. The bottom left corner, shows the *average simulation* over 64 simulated trajectories.